ACS POLYMERS Au
AN OPEN ACCESS JOURNAL OF THE AMERICAN CHEMICAL SOCIETY



pubs.acs.org/polymerau
Article

# Unraveling the Glass-like Dynamic Heterogeneity in Ring Polymer Melts: From Semiflexible to Stiff Chain

Shota Goto, Kang Kim,* and Nobuyuki Matubayasi*

Cite This: ACS Polym. Au 2023, 3, 437−446
Read Online

ACCESS | Metrics & More | Article Recommendations

**ABSTRACT:** Ring polymers are an intriguing class of polymers with unique physical properties, and understanding their behavior is important for developing accurate theoretical models. In this study, we investigate the effect of chain stiffness and monomer density on the static and dynamic behaviors of ring polymer melts using molecular dynamics simulations. Our first focus is on the non-Gaussian parameter of center-of-mass displacement as a measure of dynamic heterogeneity, which is commonly observed in glass-forming liquids. We find that the non-Gaussianity in the displacement distribution increases with the monomer density and stiffness of the polymer chains, suggesting that excluded volume interactions between centers of mass have a strong effect on the dynamics of ring polymers. We then analyze the relationship between the radius of gyration and monomer density for semiflexible and stiff ring polymers. Our results indicate that the relationship between the two varies with chain stiffness, which can be attributed to the competition between repulsive forces inside the ring and from adjacent rings. Finally, we study the dynamics of bond-breakage virtually connected between the centers of mass of rings to analyze the exchanges of intermolecular networks of bonds. Our results demonstrate that the dynamic heterogeneity of bond-breakage is coupled with the non-Gaussianity in ring polymer melts, highlighting the importance of the bond-breaking method in determining the intermolecular dynamics of ring polymer melts. Overall, our study sheds light on the factors that govern the dynamic behaviors of ring polymers.

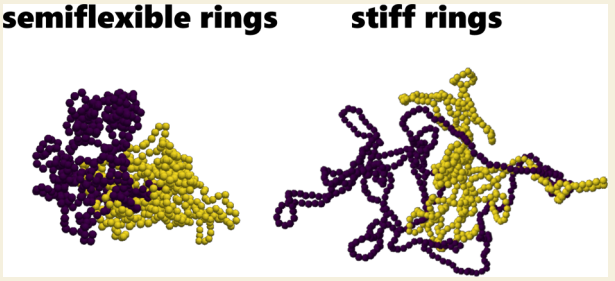


**KEYWORDS:** *ring polymers, glassy dynamics, dynamic heterogeneity, non-Gaussianity, intermolecular correlations*

## INTRODUCTION

The dynamic properties of polymer melts are governed by structural features, such as the chain length $N$ and "topological constraints" (TCs).[1,2] In linear polymer melts, entanglement is a common TC and plays a key role in describing the $N$ dependence of diffusion constant $D$. However, defining and characterizing TCs in ring polymers is still challenging due to the absence of chain ends.[3−8]

In ring polymer melts, the simple picture of TCs is that they inhibit each other's dynamics due to inter-ring "threadings".[9−12] As $N$ increases, the number of threading configurations also increases, making it more difficult for the system to find the equilibrium configuration to relax the threading. The threading event of large $N$ rings suggests a slowing-down of the dynamics, similar to the slow dynamics in glass-forming liquids, where cage effects are imposed by the local density environment.[13] The concept of a "topological glass" has been used to understand the dynamics of ring polymer melts, highlighting the unique role of TCs in these systems compared to the entanglements in linear polymers.[14−24] Interestingly, techniques such as random pinning[16,17] and activeness[21,22,24] have been introduced to enhance the glassiness in ring polymers through molecular dynamics (MD) simulations.

Dynamic heterogeneity (DH) is a key concept used to describe the significant slowing-down of glass-former liquids as they approach the glass transition temperature.[25−27] The slowing-down is accompanied by the collective structural relaxation of spatially heterogeneous regions that exceeds the molecular size.[28−31] DH is conventionally measured by the non-Gaussian parameter (NGP), i.e., the degree of the deviation from the Gaussian distribution for the molecular displacement within a given time interval.[29,32−36] The NGP was utilized to quantify the non-Gaussianity in supercooled linear polymer melts.[37−39] In addition, we conducted calculations on the NGP for linear polymer melts by MD simulations using the Kremer−Grest (KG) bead-spring model.[40] The chain lengths varied from $N$ = 5 to 400, and

Received: May 24, 2023
Revised: August 8, 2023
Accepted: August 8, 2023
Published: August 22, 2023

the monomer density was set at $\rho = 0.85$ (in the unit of $\sigma^{-3}$ by using the size of the bead $\sigma$). Our findings revealed a notable increase in the peak of the NGP as $N$ increases. This suggests that the dynamics of the system becomes spatially heterogeneous. However, note that the mechanism of non-Gaussianity in linear polymer melts is due to the enhanced mobility of chain ends, which is different from the cage effects observed in glass-forming liquids.

Michieletto et al. conducted MD simulations of ring polymers using the KG model and analyzed the center-of-mass (COM) displacement distribution.[17] They found that the non-Gaussian behavior was pronounced even in the absence of random pinning fields when the monomer density $\rho$ increased with the chain length $N = 500$. A parallel observation of the non-Gaussian behavior was also reported for ring polymers.[41] This finding is consistent with the experimental observation of poly(ethylene oxide) ring melts by Brás et al.[42] However, our previous study, which also used the same model for MD simulations of ring polymer melts, showed that the NGP remained quite small at all time regimes, even when the chain length was increased up to $N = 400$.[40] It should be noted that the chain stiffness differed between the two studies. Specifically, the bending potential $\varepsilon_\theta(1 + \cos\theta)$ (in the unit of energy scale in the Lennard-Jones potential) acts on the bending angle $\theta$ formed by three consecutive monomer beads along the polymer chain (eq 3). Michieletto et al. utilized a stiff ring chain with a bending energy of $\varepsilon_\theta = 5$ for densities up to $\rho = 0.4$. More recently, the glass-like slow dynamics has also been demonstrated at low densities by increasing the chain stiffness up to $\varepsilon_\theta = 20$.[43] By contrast, we simulated semiflexible ring chains with $\varepsilon_\theta = 1.5$ at a higher density of $\rho = 0.85$, which is the same as that used in the MD study by Halverson et al.[44−46]

Thus, there is still much to be explored regarding the influence of chain stiffness on DH in ring polymer melts. To address this gap, we performed MD simulations using the KG model by varying the $\varepsilon_\theta$ and $\rho$. Our analysis began by examining the NGP, and the analysis characterized the effect of chain stiffness on the DH in ring polymer melts. We also investigated the conformation of ring chains by analyzing the radius of gyration, as well as asphericity and prolateness based on the diagonalization of the gyration tensor. Additionally, we introduced the concept of intermolecular bonds virtually connected by ring COM positions, which enabled us to investigate the rearrangement of intermolecular connectivity of ring polymers. By combining the results obtained from these analyses, we aim to identify similarities and differences in the effects of chain stiffness and monomer density on ring polymer dynamics.

## MODEL AND METHODOLOGY

We employed MD simulations for ring polymer melts utilizing the KG model.[47] Each ring polymer was represented by $N$ monomer beads of mass $m$ and diameter $\sigma$. Our system consisted of $M$ polymer chains contained within a three-dimensional cubic box with a volume of $V$ and periodic boundary conditions. All monomer beads were subject to three types of interparticle potentials, namely, the Lennard-Jones (LJ) potential, which acted between all pairs of monomer beads,

$$U_{\mathrm{LJ}}(\boldsymbol{r}) = 4\varepsilon_{\mathrm{LJ}}\left[\left(\frac{\sigma}{r}\right)^{12} - \left(\frac{\sigma}{r}\right)^{6}\right] + C \tag{1}$$

Here $r$ and $\varepsilon_{\mathrm{LJ}}$ represent the distance between two monomer beads and the energy scale of the LJ potential, respectively. The LJ potential was truncated at the cutoff distance of $r_c = 2^{1/6}\sigma$, and the constant $C$ ensured that the potential energy shifted to zero at $r = r_c$. Additionally, two adjacent monomer beads along the chain also interacted via the bond potential

$$U_{\mathrm{bond}}(r) = -\frac{1}{2}KR_0^2\ln\left[1 - \left(\frac{r}{R_0}\right)^2\right] \tag{2}$$

for $r < R_0$, where $K$ and $R_0$ represent the spring constant and the maximum length of the bond, respectively. Note that eqs 1 and 2 define the finitely extensible nonlinear elastic (FENE) bond potential of the KG model. We adopted values of $K = 30\varepsilon_{\mathrm{LJ}}/\sigma^2$ and $R_0 = 1.5\sigma$. Lastly, we controlled the chain stiffness by incorporating a bending potential

$$U_{\mathrm{bend}}(\theta) = \varepsilon_\theta[1 - \cos(\theta - \theta_0)] \tag{3}$$

where the bending angle $\theta$ is formed by three consecutive monomer beads along the polymer chain. In this study, we explored two bending energy cases: a semiflexible chain with $\varepsilon_\theta = 1.5\varepsilon_{\mathrm{LJ}}$ and a stiff chain with $\varepsilon_\theta = 5\varepsilon_{\mathrm{LJ}}$, both with an equilibrium angle of $\theta_0 = 180°$.

We conducted MD simulations using the Large-scale Atomic/Molecular Massively Parallel Simulator (LAMMPS).[48] Hereafter, the length, energy, and time are conventionally represented in units of $\sigma$, $\varepsilon_{\mathrm{LJ}}$, and $(m\sigma^2/\varepsilon_{\mathrm{LJ}})^{1/2}$, respectively. Moreover, the temperature is also presented in units of $\varepsilon_{\mathrm{LJ}}/k_{\mathrm{B}}$, where $k_{\mathrm{B}}$ is the Boltzmann constant.

We fixed the temperature $T$, chain length $N$, and number of chains $M$ as $T = 1.0$, $N = 400$, and $M = 100$, respectively. During all simulations, the temperature was controlled by using the Nosé−Hoover thermostat, with a time step of $\Delta t = 0.01$. We varied the monomer density $\rho\sigma^3$ $(= NM\sigma^3/V)$ as 0.1, 0.3, 0.4, 0.5, and 0.55 both for the semiflexible and stiff chains. In addition, we adopted the monomer density $\rho = 0.85$ for the semiflexible chain with $\varepsilon_\theta = 1.5$, which was a common choice for MD simulations both for linear[49,50] and ring[40,44−46,51] polymers. It should be noted that a stiff chain system with $\varepsilon_\theta = 5$ displayed nematic ordering when the monomer densities exceeded $\rho = 0.55$, which is in agreement with the recent MD simulations reported in ref 52. Therefore, the system of $\varepsilon_\theta = 5$ at $\rho = 0.85$ was excluded from the analysis. For each combination of $\varepsilon_\theta$ and $\rho$ with the chain length $N = 1000$, we calculated the Kuhn length $l_k$ using $l_k = \langle R^2\rangle/l_b(N - 1)$, in linear polymers.[53] Here, $\langle R^2\rangle$ represents the mean square end-to-end distance of the chain, and $l_b \simeq 0.97$ denotes the average distance between two neighboring beads in the KG model. Another important characteristic is the entanglement length $N_e$, which we determined through the primitive path analysis.[54,55] The values of $l_k$ and $N_e$ for linear polymers with the chain length $N = 1000$ are listed in Table 1. Note that, in previous studies, $l_k$ was reported to be $l_k \simeq 2.79$ for $\varepsilon_\theta = 1.5$ at $\rho = 0.85$ and $l_k \simeq 10$ for $\varepsilon_\theta = 5$ at $\rho = 0.1$, respectively.[17,44] Additionally, $N_e$ was reported to be $N_e \simeq 28$ for $\varepsilon_\theta = 1.5$ at $\rho = 0.85$ and $N_e \simeq 40$ for $\varepsilon_\theta = 5$ at $\rho = 0.1$, respectively.[16,56] However, we encountered difficulties in estimating $N_e$ at the density $\rho = 0.1$ for both $\varepsilon_\theta = 1.5$ and 5 due to the absence of entanglement effects with $N = 1000$.


https://doi.org/10.1021/acspolymersau.3c00013
ACS Polym. Au 2023, 3, 437−446

**Table 1. Kuhn Length $l_k$ and Entanglement Length $N_e$ Are Obtained by Varying Bending Energy $\varepsilon_\theta$ and Monomer Density $\rho$ for Linear Polymers with the Chain Length $N$ = 1000**

| $\varepsilon_\theta$ | $\rho$ | $l_k$ | $N_e$ |
|---|---|---|---|
| 1.5 | 0.1 | 4.1 | *a* |
| 1.5 | 0.3 | 3.8 | 121 |
| 1.5 | 0.4 | 3.7 | 85 |
| 1.5 | 0.5 | 3.0 | 60 |
| 1.5 | 0.55 | 3.0 | 59 |
| 1.5 | 0.85 | 2.8 | 28 |
| 5 | 0.1 | 10 | *a* |
| 5 | 0.3 | 7.8 | 32 |
| 5 | 0.4 | 7.2 | 24 |
| 5 | 0.5 | 6.4 | 19 |
| 5 | 0.55 | 6.4 | 15 |

[a]No entanglement effects were observed.

## RESULTS AND DISCUSSION

### Mean Square Displacement and Non-Gaussian Parameter

We first analyzed the mean square displacement (MSD) of the COM of ring polymer chains and the NGP of the COM displacement distribution. The mean value of the even power of the COM displacement is defined by

$$\langle \Delta r_{\mathrm{COM}}^{2n}(t)\rangle = \left\langle \frac{1}{M}\sum_{m=1}^{M} |\mathbf{R}_m(t) - \mathbf{R}_m(0)|^{2n} \right\rangle, \quad (n = 1, 2, \cdots) \tag{4}$$

where $\mathbf{R}_m(t)$ represents the COM position of $m$-th polymer chain at time $t$. Here, $\langle\cdots\rangle$ denotes an average over the initial time. The second order with $n = 1$ corresponds to the MSD. Furthermore, the NGP for the COM displacement $\alpha_2(t)$ is defined by

$$\alpha_2(t) = \frac{3}{5}\frac{\langle \Delta r_{\mathrm{COM}}^4(t)\rangle}{\langle \Delta r_{\mathrm{COM}}^2(t)\rangle^2} - 1 \tag{5}$$

The NGP is a typical quantity to characterize DH in glass-forming liquids, which measures the non-Gaussianity, i.e., the degree of the deviation of the distribution function of the COM displacement from the Gaussian form during the time interval $t$.

The results of MSD and NGP are displayed in Figure 1 by changing the monomer density $\rho$ for $\varepsilon_\theta$ = 1.5 (a, c) and $\varepsilon_\theta$ = 5 (b, d), respectively. As the monomer density $\rho$ increased, the diffusion of ring polymer chains significantly slowed for both $\varepsilon_\theta$ = 1.5 and 5. Moreover, at higher densities, the MSD exhibits a subdiffusive behavior with $\langle \Delta r_{\mathrm{COM}}^2(t)\rangle \sim t^{3/4}$, followed by diffusion behavior observed at displacements larger than mean square gyration of radius $\langle R_g^2\rangle$. The mean square radius of gyration $\langle R_g^2\rangle$ will be discussed in the next subsection with respect to Figure 2. The COM diffusion constant $D$ was determined from $D = \lim_{t\to\infty} \langle \Delta r_{\mathrm{COM}}^2(t)\rangle/6t$. The monomer

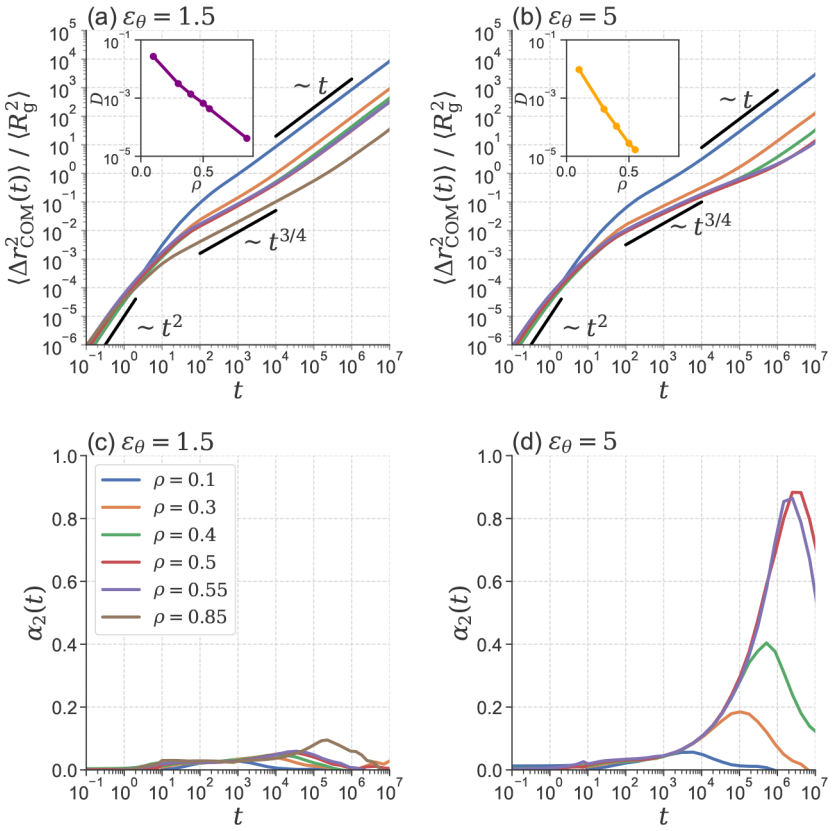


**Figure 1.** Monomer density $\rho$ dependence of MSD $\langle \Delta r_{\mathrm{COM}}^2(t)\rangle$ and NGP $\alpha_2(t)$ for $\varepsilon_\theta$ = 1.5 (a, c) and for $\varepsilon_\theta$ = 5 (b, d), respectively. Note that the MSD is scaled by the mean square gyration of radius $\langle R_g^2\rangle$. In (a) and (b), the ballistic, subdiffusive, and diffusive behaviors, $\langle \Delta r_{\mathrm{COM}}^2(t)\rangle \sim t^\alpha$, are represented by black lines with $\alpha$ = 2, 3/4, and 1, respectively. Insets of (a) and (b): semilog plots of the diffusion constant $D$ as a function of the monomer density $\rho$. Note that monomer density $\rho$ = 0.85 was analyzed only for $\varepsilon_\theta$ = 1.5.



https://doi.org/10.1021/acspolymersau.3c00013
ACS Polym. Au 2023, 3, 437−446

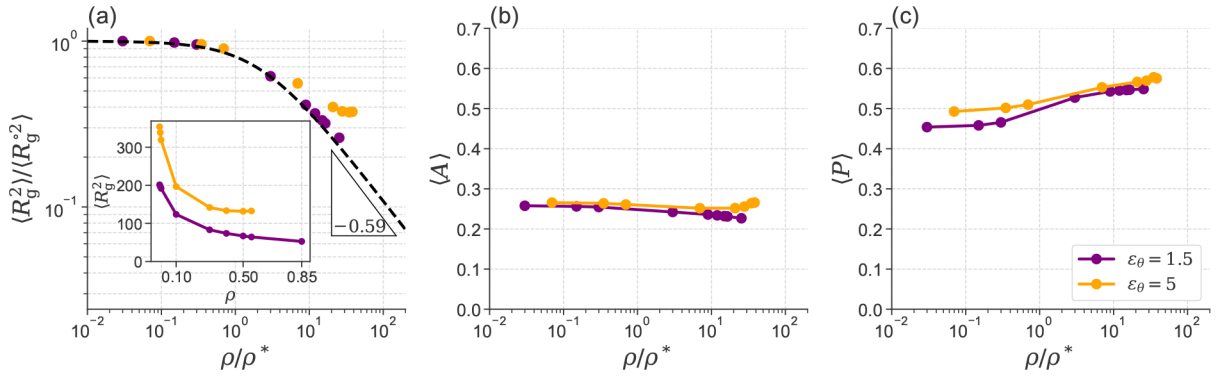


**Figure 2.** Monomer density $\rho$ scaled by the overlap density $\rho^*$ dependence of chain conformation characteristics: (a) mean square radius of gyration $\langle R_g^2\rangle/\langle R_g^{\circ 2}\rangle$, (b) asphericity $A$, and (c) prolateness $P$. In (a), the mean square radius of gyration is normalized by $\langle R_g^{\circ 2}\rangle$, which represents the mean square radius of gyration at a density of $\rho = 0.001$. The raw data of $\langle R_g^2\rangle$ as a function of $\rho$ are also shown in the inset of panel (a). The black dotted line in (a) is the master curve, $\langle R_g^2\rangle/\langle R_g^{\circ 2}\rangle = [1 + 0.45(\rho/\rho^*)]^{-0.59}$. In each panel, the density is scaled density $\rho^* = 3N/(4\pi\langle R_g^{\circ 2}\rangle^{3/2})$.

density $\rho$ dependence of $D$ for $\varepsilon_\theta = 1.5$ and 5 is shown in the insets of Figure 1(a) and (b), respectively. The reduction in diffusion was more pronounced for the stiff chains with $\varepsilon_\theta = 5$ compared to semiflexible chains with $\varepsilon_\theta = 1.5$ at time scales corresponding to the onset of the diffusion process at the same monomer density. These observations are consistent with the calculations by Michieletto et al.[17] and Halverson et al.[45]

As demonstrated in Figure 1(c), the NGP's value of semiflexible ring chains with $\varepsilon_\theta = 1.5$ remained relatively small ($\alpha_2(t) \lesssim 0.1$) at all investigated times and densities. This suggests that the distribution of the COM displacement $|\boldsymbol{R}_m(t) - \boldsymbol{R}_m(0)|$ follows a Gaussian distribution, which was previously reported in our work.[40] The observation of Gaussian behavior in semiflexible ring polymers, even at the dense monomer density of $\rho = 0.85$, is noteworthy and provides a unique perspective on the dynamics of ring polymers. By contrast, for stiff ring chains, the increase in $\alpha_2(t)$ was more significant, showing peaks in a long-time regime that approximately corresponded to the onset time scale of the diffusive behavior with $\langle \Delta r_{COM}^2(t)\rangle \sim t$, as demonstrated in Figure 1(b) and (d). Namely, the DH was found to be more pronounced in stiff ring chains with $\varepsilon_\theta = 5$, similar to common observations in glass-forming liquids. An analogous glass-like DH was reported by Michieletto et al., who analyzed the displacement distribution of stiff ring chains with $\varepsilon_\theta = 5$ up to $\rho = 0.4$ with $N = 500$.[17] Therefore, the contracting observations in the NGP call for further investigations into the COM mobility, which could entail significant differences between semiflexible and stiff ring chains.

## Conformation of the Ring Chains: Radius of Gyration, Asphericity, and Prolateness

It is important to examine the details regarding the conformation of rings and its relationship with the DH both for semiflexible and stiff chains. The radius of gyration provides a measure of the size of the polymer chains. To gain a more sophisticated understanding of the shapes, the principal components of the gyration tensor $\mathbf{I}$ can be utilized, which allows for examination of the asphericity and prolateness of the polymer chains.[57−60] The gyration tensor for each ring chain is defined as $I_{\alpha\beta} = N^{-1}\sum_{i=1}^{N}\sum_{j=1}^{N}(\alpha_i - \alpha_j)(\beta_i - \beta_j)$, where $\alpha$ represents the $\alpha$ element of the $i$-th bead with $\alpha, \beta$ $(= x, y, z)$. Here, the square radius of gyration $R_g^2$ can be calculated as the summation of the eigenvalues $\lambda_i$ $(i = 1, 2, 3)$ of the gyration tensor $\mathbf{I}$ as $R_g^2 = \lambda_1 + \lambda_2 + \lambda_3$, where the principal axes of inertia are chosen such that the diagonal elements are ordered as $\lambda_1 \geq \lambda_2 \geq \lambda_3$. Furthermore, the asphericity $A$ and prolateness $P$ were calculated from the following equations:

$$A = \frac{(\lambda_1 - \lambda_2)^2 + (\lambda_1 - \lambda_3)^2 + (\lambda_2 - \lambda_3)^2}{2(\lambda_1 + \lambda_2 + \lambda_3)^2} \tag{6}$$

$$P = \frac{(2\lambda_1 - \lambda_2 - \lambda_3)(2\lambda_2 - \lambda_1 - \lambda_3)(2\lambda_3 - \lambda_1 - \lambda_2)}{2(\lambda_1^2 + \lambda_2^2 + \lambda_3^2 - \lambda_1\lambda_2 - \lambda_1\lambda_3 - \lambda_2\lambda_3)^{3/2}} \tag{7}$$

The asphericity takes on values of $0 \leq A \leq 1$, where $A = 0$ corresponds to a spherically symmetric object and $A = 1$ corresponds to a polymer that is fully extended to form a rod shape. The prolateness $P$ is bounded between −1 and 1, where $P = -1$ represents a fully oblate object such as a disk and $P = 1$ represents a prolate object in the shape of a rod. The gyration tensor was calculated for each chain, and the time evolutions of $R_g^2$, $A$, and $P$ were computed. The mean values $\langle R_g^2\rangle$, $\langle A\rangle$, and $\langle P\rangle$ were evaluated by taking the average of these quantities over the time series data for each chain. It should be noted that the analysis of the gyration tensor was performed in various simulations of ring polymers.[60−68]

Reigh and Yoon reported a universal scaling behavior of $\langle R_g^2\rangle \sim \rho^{-0.59}$ for long ring polymers by Monte Carlo simulation of a lattice model.[66] This exponent of −0.59 is significantly different from the value of −0.25 observed for linear polymers, which was a well-established prediction based on scaling arguments. This observation suggests that ring chains form more compact conformations than linear chains. More recently, Cai et al. performed MD simulations of ring polymers using the KG model by varying chain lengths $N$ up to 5120 and reported the same scaling behavior of $\langle R_g^2\rangle \sim \rho^{-0.59}$.[67] The master curve was then proposed heuristically and given by

$$\langle R_g^2\rangle/\langle R_g^{\circ 2}\rangle = [1 + 0.45(\rho/\rho^*)]^{-0.59} \tag{8}$$

where $\langle R_g^{\circ 2}\rangle$ denotes the mean square radius of gyration in the dilute solutions. In addition, $\rho^*$ corresponds to the overlap density defined by $\rho^* = 3N/(4\pi\langle R_g^{\circ 2}\rangle^{3/2})$. They also compared their simulation results with available experimental data and found good agreement between simulations and experiments. Note that the ring polymer chains in their


https://doi.org/10.1021/acspolymersau.3c00013
ACS Polym. Au 2023, 3, 437−446

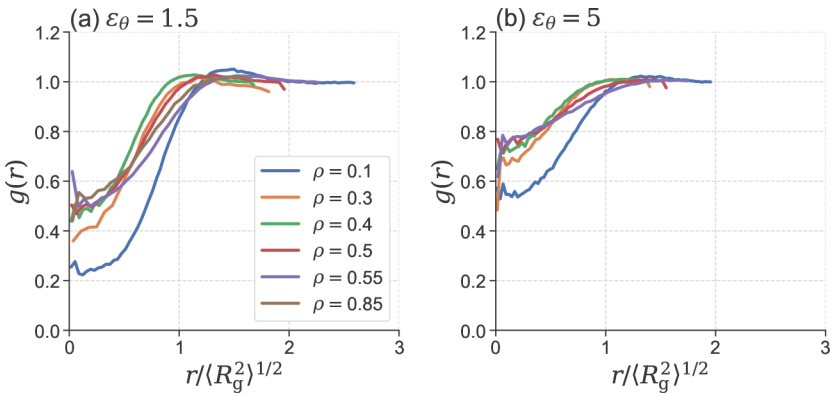


**Figure 3.** Radial distribution function $g(r)$ for COM of ring polymers as a function of the scaled distance $r/\langle R_g^2\rangle^{1/2}$. Results are shown for $\varepsilon_\theta = 1.5$ (a) and $\varepsilon_\theta = 5$ (b).

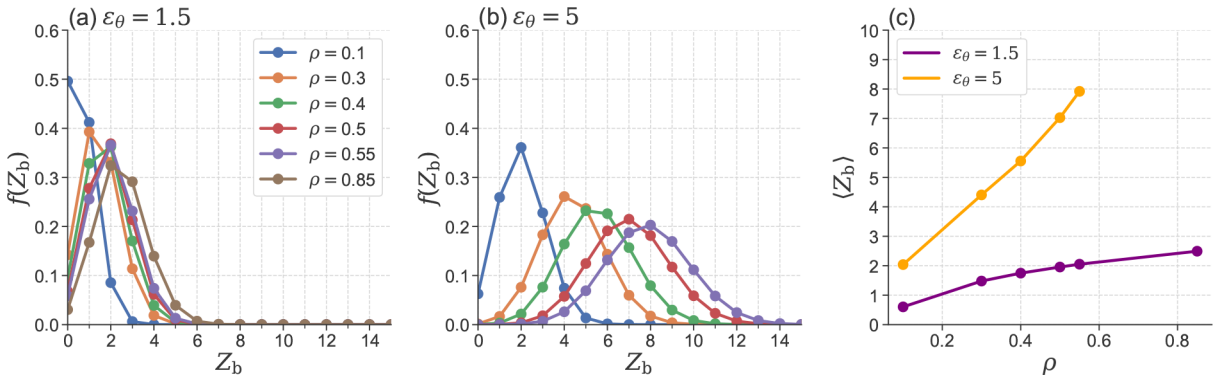


**Figure 4.** Probability distributions of the number of virtual bonds, $f(Z_b)$, for ring polymers of $\varepsilon_\theta = 1.5$ (a) and $\varepsilon_\theta = 5$ (b). The virtual bonds are defined based on eq 9. Panel (c) shows the monomer density $\rho$ dependence of the mean value of $Z_b$.

simulations were fully flexible, because they did not incorporate any bending potentials.

Figure 2(a) shows the relative mean square radius of gyration $\langle R_g^2\rangle/\langle R_g^{\circ 2}\rangle$ as a function of scaled density $\rho/\rho^*$. We estimated $\langle R_g^{\circ 2}\rangle$ as the value of mean square radius of gyration $\langle R_g^2\rangle$ both for semiflexible and stiff chains at a density of $\rho$ = 0.001. This density corresponds to a sufficiently low scaled density ($\rho/\rho^* < 10^{-1}$), making it appropriate to consider $\rho$ = 0.001 as a dilute solution both for semiflexible and stiff ring polymers. The data for semiflexible rings with $\varepsilon_\theta = 1.5$ follow the master curve given by eq 8. However, a deviation from eq 8 was observed for stiff rings with $\varepsilon_\theta = 5$, indicating that $\langle R_g^2\rangle$ of stiff ring chains decreases slower than that of semiflexible ring chains as the density is increased beyond $\rho/\rho^* \gtrsim 10$. The inset in Figure 2 (a) shows the density $\rho$ dependence of the mean square radius of gyration $\langle R_g^2\rangle$. This represents that the stiff rings are larger than the semiflexible ones in all densities $\rho$.

Figure 2(b) and (c) show the average asphericity $\langle A\rangle$ and average prolateness $\langle P\rangle$, respectively, as functions of $\rho/\rho^*$. Interestingly, we found that the values of $\langle A\rangle$ and $\langle P\rangle$ approached saturation regardless of the bending energy $\varepsilon_\theta$. In particular, the relatively small values of $\langle A\rangle \simeq 0.2$–$0.3$ suggest that the ring polymer adopts globular conformations, which remain valid across the densities examined. However, slightly large values of $\langle P\rangle \simeq 0.5$ indicate that the rings extend moderately in the direction of the longest inertia axis. These imply that the shape of the rings is mostly spherical and relatively insensitive to both $\varepsilon_\theta$ and $\rho$, provided that the chain length is sufficiently long compared to the Kuhn length scale, which was quantified for linear polymers with $N$ = 1000 (see Table 1).

## Interpenetration of Ring Chains

As shown in Figure 2, while the shape of the polymer remained largely unchanged on average, there was an increase in the mean square radius of gyration $\langle R_g^2\rangle$ when the chain stiffness increased to $\varepsilon_\theta$ = 5. This suggests that the intermolecular connectivity of ring chains may differ significantly between semiflexible and stiff chains. To explore this further, we calculated the radial distribution function for the COM of ring chains $g(r)$, and the results are presented in Figure 3 as a function of the scaled length of $r/\langle R_g^2\rangle^{1/2}$.

As observed in Figure 3, $g(r)$ allowed us to characterize the degree of interpenetration of ring polymers. In fact, we did not observe a pronounced peak of $g(r)$ but instead found finite values at the length scale of $r < \langle R_g^2\rangle^{1/2}$, indicating that there is some degree of interpenetration between the ring chains. The $g(r)$ became broader with increasing monomer density, suggesting that the chains are less separated from each other. Similar results of $g(r)$ were reported for flexible chains without the bending potential by Cai et al.[67] Additionally, as shown in Figure 3(b), the degree of the interpenetration became more significant as the bending energy increased to $\varepsilon_\theta$ = 5. This observation is consistent with the larger mean square radius of gyration $\langle R_g^2\rangle$ of stiff rings with $\varepsilon_\theta$ = 5 compared to that of semiflexible rings of $\varepsilon_\theta$ = 1.5 at the same monomer density $\rho$. The extent of interpenetration needs to be stronger when the ring is "larger". The difference in $\langle R_g^2\rangle$ is also evident in Figure


https://doi.org/10.1021/acspolymersau.3c00013
ACS Polym. Au 2023, 3, 437−446

2, where the curve for $\varepsilon_\theta = 5$ is shifted to higher values of $\rho/\rho^*$ compared to $\varepsilon_\theta = 1.5$. These results suggest that the competition between repulsive forces inside the ring and those from adjacent rings plays a crucial role in determining the loop structure. While sufficiently semiflexible polymers tend to be more compact because the repulsion between neighboring rings overcomes the monomer bead repulsion inside a single chain, the stiff polymers tend to expand due to the long Kuhn length (see Table 1), leading to the interpenetration of rings.

To analyze the number of intermolecular connectivity, we considered virtually connected bonds between the COM of ring chains. In particular, for two ring polymers $i$ and $j$ with the COM positions $\mathbf{r}_i$ and $\mathbf{r}_j$, they were considered to be virtually bonded if

$$r_{ij} < A_1\langle R_g^2\rangle^{1/2} \tag{9}$$

with the value of $A_1 = 1$. Here, $r_{ij} = |\mathbf{R}_i - \mathbf{R}_j|$ is the distance between these COMs. For each polymer, the number of virtual bonds $Z_b$, which represents the static coordination number, was counted. Figure 4 depicts the probability distribution $f(Z_b)$ for ring polymers of $\varepsilon_\theta = 1.5$ (a) and $\varepsilon_\theta = 5$ (b) at varying density $\rho$. In the case of semiflexible rings with $\varepsilon_\theta = 1.5$, the peak was observed at around 2 for most densities, except for $\rho = 0.1$, where $Z_b$ was predominantly 0, indicating that each ring chain was mostly isolated and did not correlate with each other. However, for stiff rings with $\varepsilon_\theta = 5$, we observed progressive increases in the peak position and width of $f(Z_b)$ as density $\rho$ increased. The monomer density $\rho$ dependence of the mean value of $Z_b$ is shown in Figure 4(c). Here, $\langle Z_b\rangle$ can be evaluated by

$$\langle Z_b\rangle = \int_0^{\langle R_g^2\rangle^{1/2}} 4\pi r^2\left(\frac{\rho}{N}\right)g(r)\,dr \tag{10}$$

In cases of $g(r) = 1$ and $\langle R_g^2\rangle \sim \rho^{-0.6}$, $\langle Z_b\rangle$ may exhibit a scaling behavior of $\langle Z_b\rangle \sim \rho\langle R_g^2\rangle^{3/2} \sim \rho^{0.1}$ at a fixed chain length $N$. This suggests that $\langle Z_b\rangle$ increases slowly as the density increases. However, the presence of $g(r) < 1$ for $r < \langle R_g^2\rangle^{1/2}$, as observed in Figure 3 both for $\varepsilon_\theta = 1.5$ and 5, leads to the deviation from the expected $\langle Z_b\rangle \sim \rho^{0.1}$. Notably, as shown in Figure 2(a), $\langle R_g^2\rangle$ of $\varepsilon_\theta = 5$ does not follow the $\rho^{-0.6}$ scaling, resulting in a more pronounced increase in $\langle Z_b\rangle$ with increasing the density.

Moreover, the spatial distribution of intermolecular connectivity is visualized in Figure 5. For semiflexible ring polymers with $\varepsilon_\theta = 1.5$, bonds describing the connectivity of COM are sparse irrespective of the monomer density $\rho$. In contrast, as the density increases, ring polymers with higher stiffness ($\varepsilon_\theta = 5$) exhibit stronger percolation, indicating a more interconnected network bond. It is noteworthy that there exists a critical coordination number around 3, beyond which the linked ring polymers percolate through the entire system.[69]

## Rearrangements of Intermolecular Connectivity

To examine rearrangements of intermolecular connectivity of ring polymers, we analyzed the time evolution of virtual bonds. This reflects the exchange of initially bonded neighbors because the COM motion breaks old bonds and forms new ones. Although the average coordination number $\langle Z_b\rangle$ may remain constant, the neighboring COMs will be replaced with new ones, thereby reshaping the cages around a tagged COM. A similar methodology, known as the bond-breakage method, is used to study the DH observed in glass-forming liquids.[30,70−73]

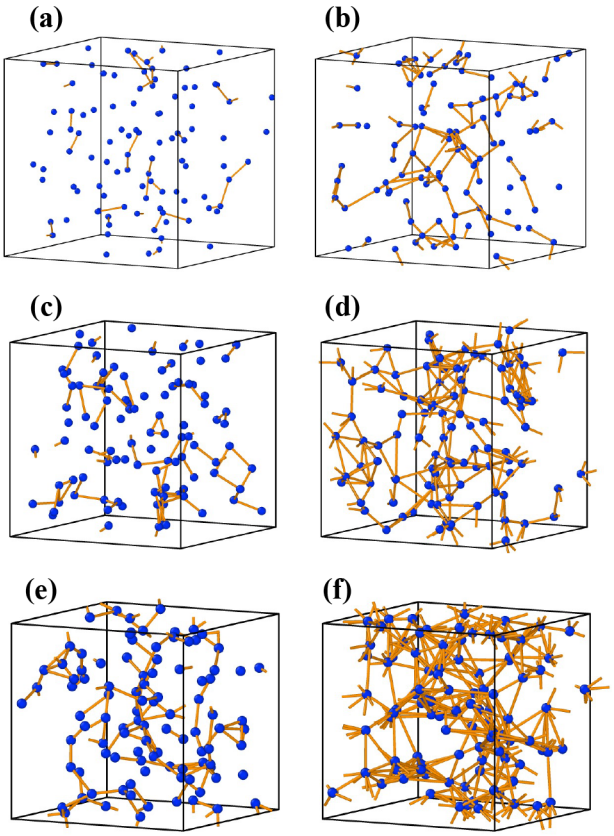


**Figure 5.** Visualization of virtual bonds (yellow lines) between the COM of rings (blue spheres) for $\varepsilon_\theta = 1.5$ (a, c, and e) and $\varepsilon_\theta = 5$ (b, d, and f). The monomer density $\rho$ increases as $\rho = 0.1$, 0.3, and 0.5 from top to bottom.

The virtual bond between two polymers $i$ and $j$ which had been counted to be formed at an initial time 0 through eq 9 was considered broken when

$$r_{ij}(t) > A_2\langle R_g^2\rangle^{1/2} \tag{11}$$

after a time interval of $t$. To ensure bond-breaking that is insensitive to thermal fluctuations, the threshold value of $A_2 = 1.2$ was set slightly larger than $A_1 = 1$. The total number of surviving bonds, $N_b(t)$, was calculated as the number of bonds at time 0 counted with eq 9 subtracted by that through eq 11. The bond correlation function, $F_b(t) = \langle N_b(t)/N_b(0)\rangle$, was obtained by averaging over the configurations at $t = 0$. Figure 6 shows the results of $F_b(t)$ for $\varepsilon_\theta = 1.5$ (a) and $\varepsilon_\theta = 5$ (b), respectively. The characteristic time scale of $F_b(t)$ is related to that of the rearrangement of the local coordination by neighboring COMs, according to the definition of the bond. The $F_b(t)$ was fitted to the stretched exponential function $F_b(t) = \exp[-(t/\tau_b)^\beta]$ where the exponent $\beta$ represents the degree of the deviation from the exponential decay with $\beta = 1$. The average relaxation time $\langle\tau_b\rangle$ was then calculated from $\langle\tau_b\rangle = \int_0^\infty F_b(t)\,dt$, and estimated by $\langle\tau_b\rangle = (\tau_b/\beta)\Gamma(1/\beta)$ with the Gamma function $\Gamma(\cdots)$. Figure 6(c) shows $\langle\tau_b\rangle$ as a function of monomer density $\rho$. Our results demonstrate the increase in the average relaxation time $\langle\tau_b\rangle$ of $F_b(t)$ as monomer density $\rho$ increased, for both $\varepsilon_\theta = 1.5$ and $\varepsilon_\theta = 5$. The increase in $\langle\tau_b\rangle$ apparently obeys an exponential trend as a function of $\rho$,


https://doi.org/10.1021/acspolymersau.3c00013
ACS Polym. Au 2023, 3, 437−446

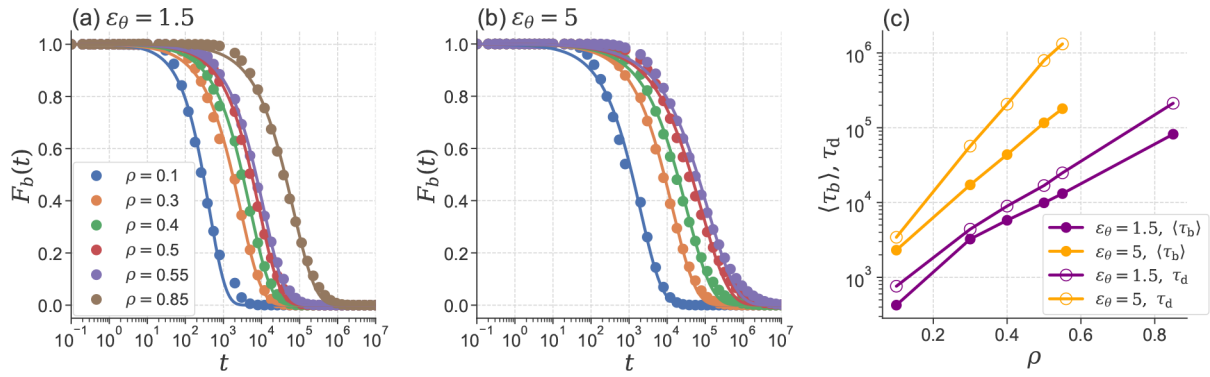


**Figure 6.** Monomer density dependence of the bond correlation function $F_b(t)$ for $\varepsilon_\theta = 1.5$ (a) and $\varepsilon_\theta = 5$ (b). The solid line represents the fitting result obtained using the stretched exponential function, $F_b(t) \approx \exp[-(t/\tau_b)^\beta]$. Panel (c) shows the monomer density $\rho$ dependence of the average relaxation time $\langle\tau_b\rangle$ of the bond correlation function $F_b(t)$ and the diffusion time $\tau_d = \langle R_g^2\rangle/6D$.

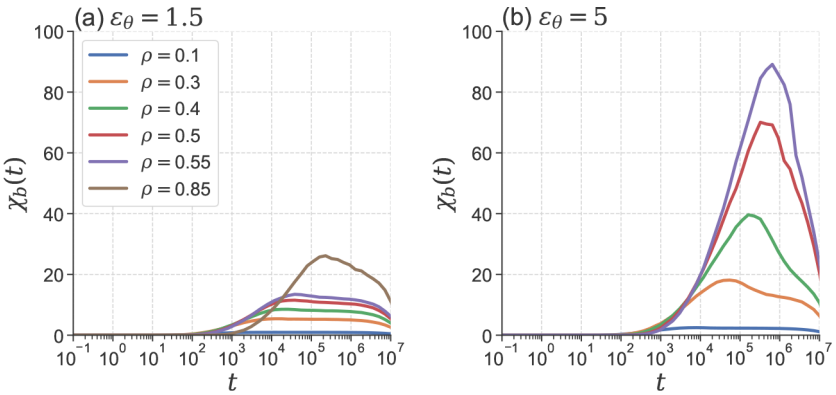


**Figure 7.** Monomer density dependence of the dynamic susceptibility of bond-breakage $\chi_b(t)$ for $\varepsilon_\theta = 1.5$ (a) and $\varepsilon_\theta = 5$ (b).

except at the dilute density of $\rho = 0.1$ for $\varepsilon_\theta = 1.5$, where the average coordination number $\langle Z_b\rangle$ is less than 1, indicating that the polymer rings are nearly isolated (see Figure 4(c)). Furthermore, we observed a more pronounced increase in $\langle\tau_b\rangle$ for stiff ring polymers with $\varepsilon_\theta = 5$, which is in accordance with the monomer density $\rho$ dependence of $\langle Z_b\rangle$ (see again Figure 4(c)).

Another significant time scale to consider is the diffusion time, $\tau_d$, defined as $\tau_d = \langle R_g^2\rangle/6D$, which corresponds to the time at which the MSD reaches the length scale of the mean square radius of gyration $\langle R_g^2\rangle$. The monomer density dependence of $\tau_d$ is illustrated in Figure 6(c). It is observed that, for semiflexible rings with $\varepsilon_\theta = 1.5$, $\tau_d$ increases in a similar manner to $\langle\tau_b\rangle$, while for stiff rings with $\varepsilon_\theta = 5$, $\tau_d$ exhibits a significant increase and becomes decoupled from $\langle\tau_b\rangle$ as the density $\rho$ increases. These observations suggest the COM diffusion of stiff rings is not solely driven by local bond rearrangements but requires a cooperative mechanism.

We then examined the collective effects of bond rearrangements in ring polymers. For this purpose, the dynamic susceptibility of bond-breakage was calculated by the fluctuation function of the number of broken bonds at different time intervals, $t$.[71] The number of the breakage-bond $B_i(t)$ between two times 0 and $t$ for the $i$-th polymer was counted as the difference between $N_b(t)$ and $N_b(0)$ on the basis of the conditions given in eqs 9 and 11. The degree of bond-breakage correlations can be characterized by the susceptibility $\chi_b(t)$, which is defined as

$$\chi_b(t) = \frac{1}{M}\left\langle \sum_{i=1}^{M}\sum_{j=1}^{M} \delta B_i(t)\delta B_j(t) \right\rangle \tag{12}$$

where $\delta B_i(t) = B_i(t)/2 - \langle B(t)\rangle$ represents the deviation from the average number of broken bonds. The average number of broken bonds can be estimated as $\langle B(t)\rangle = \langle\sum_{i=1}^{M} B_i(t)/2\rangle/M$. Note that the factor of 1/2 avoided double-counting of the bond-breakage between polymers $i$ and $j$. Figure 7 illustrates the susceptibility of bond-breakage, $\chi_b(t)$, for different values of $\varepsilon_\theta$ and $\rho$. For semiflexible rings with $\varepsilon_\theta = 1.5$, the $\chi_b(t)$ shows relatively small values, whereas the peak of $\chi_b$ became pronounced ($\chi_b \sim 30$) at the highest density $\rho = 0.85$ investigated. In contrast, for stiff rings with $\varepsilon_\theta = 5$, the peaks show significant development with increasing monomer density, particularly at the time regimes where the MSD nearly reaches diffusive behavior. At a density of $\rho = 0.55$, the peak height reaches $\chi_b \sim 90$. Therefore, the observed NGP behavior in Figure 1(c) and (d) is related to DH, which is also characterized by the bond-breakage susceptibility, $\chi_b(t)$. Interestingly, the results of $\alpha_2(t)$ and $\chi_b(t)$ suggest that ring polymers with $\varepsilon_\theta = 1.5$ exhibit spatial homogeneous dynamics, even in the subdiffusion regime. From this perspective, the interchain interactions in semiflexible ring polymer melts display notable characteristics, while stiff ring polymer melts exhibit interactions reminiscent of "entanglements" in linear polymer melts.

Mei et al. have recently developed the polymer interaction site model (PRISM) as a microscopic theory for dense ring


https://doi.org/10.1021/acspolymersau.3c00013
ACS Polym. Au 2023, 3, 437−446

polymer melts.[74,75] This theory proposes a partially interpenetrating, two-step fractal structure model for each ring chain and provides a master curve for the chain length $N$ dependence of the COM diffusion constant $D$. Although the PRISM theory has shown good agreement with MD simulations data for semiflexible ring polymers with $\varepsilon_\theta$ = 1.5,[45] deviations from the master curve have been observed for stiff rings of $\varepsilon_\theta$ = 5.[17] To gain a deeper understanding of the underlying mechanism of emergence of DH in ring polymer melts, a combined effort between theory and simulation may be necessary. In particular, our MD simulation results analyzing DH can provide insights into the deviation from the master curves reported in ref 75 and may facilitate a generalization of the theory by incorporating an activated hopping process.[76]

## CONCLUSION

In conclusion, our MD simulations of ring polymer melts using the KG model have provided insights into the dynamics of semiflexible and stiff ring chains. By analyzing the NGP in the distribution of the COM displacement, we have found that more stiff ring chains exhibit a peak in the NGP in long-time regimes, which increases with the monomer density. This suggests that the dynamics of stiff ring chains are affected by strong intermolecular interactions and that the motions of the COMs are correlated with each other. In contrast, more flexible ring polymers exhibit relatively small non-Gaussianity, indicating that the COM mobility is almost uncorrelated with those of the others. The difference in non-Gaussianity between the two types of ring polymers suggests that the nature of the intermolecular interactions changes significantly depending on the degree of chain stiffness.

The behavior of the radius of gyration $R_g$ in relation to $\rho$ depends on the stiffness of the ring polymer chains. In the case of more semiflexible rings, the $R_g$ follows a master curve described by eq 8. However, this curve does not apply to stiff ring polymer melts. The deviation from the master curve can be explained by the competition between the shrinkage caused by the excluded volume of neighboring polymers and the expansion due to the chain stiffness. Specifically, semiflexible ring polymers tend to adopt a compact globule conformation due to the excluded volume interaction with their neighbors, while more stiff rings expand due to the long Kuhn length.

We have also analyzed the dynamics of bond-breakage between the COM of rings defined by using the averaged radius of gyration, $\langle R_g^2 \rangle^{1/2}$. The network of virtual bonds in stiff rings is percolating, while those in semiflexible rings are sparsely distributed. Furthermore, the results for the dynamic susceptibility of bond-breakage are consistent with the non-Gaussianity in the displacement distribution, indicating that the DH of bond-breakage is coupled with the non-Gaussianity in diffusion in ring polymer melts. In addition, it is crucial to investigate the dynamics of ring-linear blend melts.[55,77−80] In practical terms, the analysis of the bond-breakage is particularly well-suited for this system, enabling the assessment of the interconnectivity dynamics of polymer chain COMs.

Threading is commonly discussed in ring polymer melts, but the relationship with bond-breakage dynamics remains unclear. Further investigation into the properties of threading in ring polymer melts with varying chain stiffness is warranted. Finally, we have found that semiflexible ring polymers exhibit subdiffusion yet (near-)Gaussian distribution that is contrast to linear and stiff ring chains. We suggest that the microscopic theory based on PRISM for ring polymer melts will be useful for understanding the diffusion mechanisms of these systems. Drawing on another crucial insight from ref 69, we put forward the notion that the value of $\langle Z_b \rangle$ = 3 acts as a threshold for the percolation of virtual bond networks and the emergence of DH in ring polymers. To gain deeper insights, further analysis is required, including the cluster size distribution by varying the chain stiffness $\varepsilon_\theta$ and extending the study to a longer chain length $N$. Currently, we are pursuing the application of persistent homology analysis to explore this perspective further.[11]

## AUTHOR INFORMATION


### Corresponding Authors

**Kang Kim** − *Division of Chemical Engineering, Department of Materials Engineering Science, Graduate School of Engineering Science, Osaka University, Osaka 560-8531, Japan*; orcid.org/0000-0002-7047-3183; Email: kk@cheng.es.osaka-u.ac.jp

**Nobuyuki Matubayasi** − *Division of Chemical Engineering, Department of Materials Engineering Science, Graduate School of Engineering Science, Osaka University, Osaka 560-8531, Japan*; orcid.org/0000-0001-7176-441X; Email: nobuyuki@cheng.es.osaka-u.ac.jp

### Author

**Shota Goto** − *Division of Chemical Engineering, Department of Materials Engineering Science, Graduate School of Engineering Science, Osaka University, Osaka 560-8531, Japan*

Complete contact information is available at: https://pubs.acs.org/10.1021/acspolymersau.3c00013


### Author Contributions

CRediT: **Shota Goto** data curation (lead), investigation (lead), software (lead), writing-original draft (lead); **Kang Kim** conceptualization (lead), funding acquisition (equal), supervision (lead), writing-review & editing (equal); **Nobuyuki Matubayasi** conceptualization (equal), funding acquisition (equal), supervision (equal), writing-review & editing (equal).

### Notes

The authors declare no competing financial interest.

## ACKNOWLEDGMENTS

The authors would like to thank Dr. Takenobu Nakamura for valuable discussions. This work was supported by JSPS KAKENHI Grant-in-Aid Grant Nos. JP22H04542 and JP22K03550. This work was also partially supported by JST, the establishment of university fellowships towards the creation of science technology innovation, Grant No. JPMJFS2125. We acknowledge support from the Fugaku Supercomputing Project (Nos. JPMXP1020230325 and JPMXP1020230327) and the Data-Driven Material Research Project (No. JPMXP1122714694) from the Ministry of Education, Culture, Sports, Science, and Technology. The numerical calculations were performed at Research Center of Computational Science, Okazaki Research Facilities, National Institutes of Natural Sciences (Project: 23-IMS-C052) and at the Cybermedia Center, Osaka University.



https://doi.org/10.1021/acspolymersau.3c00013
ACS Polym. Au 2023, 3, 437−446

## REFERENCES


(1) de Gennes, P. G. *Scaling Concepts in Polymer Physics*; Cornell University Press, 1979.
(2) Doi, M.; Edwards, S. F. *The Theory of Polymer Dynamics*; International Series of Monographs on Physics; Oxford University Press, 1986.
(3) Cates, M.; Deutsch, J. Conjectures on the Statistics of Ring Polymers. *J. Phys. (Paris)* **1986**, *47*, 2121−2128.
(4) Grosberg, A.; Rabin, Y.; Havlin, S.; Neer, A. Crumpled Globule Model of the Three-Dimensional Structure of DNA. *Europhys. Lett.* **1993**, *23*, 373−378.
(5) Sakaue, T. Ring Polymers in Melts and Solutions: Scaling and Crossover. *Phys. Rev. Lett.* **2011**, *106*, 167802.
(6) Halverson, J. D.; Smrek, J.; Kremer, K.; Grosberg, A. Y. From a Melt of Rings to Chromosome Territories: The Role of Topological Constraints in Genome Folding. *Rep. Prog. Phys.* **2014**, *77*, 022601.
(7) Ge, T.; Panyukov, S.; Rubinstein, M. Self-Similar Conformations and Dynamics in Entangled Melts and Solutions of Nonconcatenated Ring Polymers. *Macromolecules* **2016**, *49*, 708−722.
(8) Kim, J.; Kim, J. M.; Baig, C. Intrinsic Structure and Dynamics of Monolayer Ring Polymer Melts. *Soft Matter* **2021**, *17*, 10703−10715.
(9) Müller, M.; Wittmer, J. P.; Cates, M. E. Topological Effects in Ring Polymers: A Computer Simulation Study. *Phys. Rev. E* **1996**, *53*, 5063−5074.
(10) Smrek, J.; Grosberg, A. Y. Minimal Surfaces on Unconcatenated Polymer Rings in Melt. *ACS Macro Lett.* **2016**, *5*, 750−754.
(11) Landuzzi, F.; Nakamura, T.; Michieletto, D.; Sakaue, T. Persistence Homology of Entangled Rings. *Phys. Rev. Research* **2020**, *2*, 033529.
(12) Staňo, R.; Likos, C. N.; Smrek, J. To Thread or Not to Thread? Effective Potentials and Threading Interactions between Asymmetric Ring Polymers. *Soft Matter* **2022**, *19*, 17−30.
(13) Donth, E.-J. *The Glass Transition: Relaxation Dynamics in Liquids and Disordered Materials*; Springer Berlin Heidelberg, 2001.
(14) Lo, W.-C.; Turner, M. S. The Topological Glass in Ring Polymers. *EPL* **2013**, *102*, 58005.
(15) Lee, E.; Kim, S.; Jung, Y. Slowing Down of Ring Polymer Diffusion Caused by Inter-Ring Threading. *Macromol. Rapid Commun.* **2015**, *36*, 1115−1121.
(16) Michieletto, D.; Turner, M. S. A Topologically Driven Glass in Ring Polymers. *Proc. Natl. Acad. Sci. U.S.A.* **2016**, *113*, 5195−5200.
(17) Michieletto, D.; Nahali, N.; Rosa, A. Glassiness and Heterogeneous Dynamics in Dense Solutions of Ring Polymers. *Phys. Rev. Lett.* **2017**, *119*, 197801.
(18) Michieletto, D.; Marenduzzo, D.; Orlandini, E.; Turner, M. Ring Polymers: Threadings, Knot Electrophoresis and Topological Glasses. *Polymers* **2017**, *9*, 349.
(19) Sakaue, T. Topological Free Volume and Quasi-Glassy Dynamics in the Melt of Ring Polymers. *Soft Matter* **2018**, *14*, 7507−7515.
(20) Gómez, L. R.; García, N. A.; Pöschel, T. Packing Structure of Semiflexible Rings. *Proc. Natl. Acad. Sci. U.S.A.* **2020**, *117*, 3382−3387.
(21) Smrek, J.; Chubak, I.; Likos, C. N.; Kremer, K. Active Topological Glass. *Nat. Commun.* **2020**, *11*, 26.
(22) Chubak, I.; Likos, C. N.; Kremer, K.; Smrek, J. Emergence of Active Topological Glass through Directed Chain Dynamics and Nonequilibrium Phase Segregation. *Phys. Rev. Research* **2020**, *2*, 043249.
(23) Michieletto, D.; Sakaue, T. Dynamical Entanglement and Cooperative Dynamics in Entangled Solutions of Ring and Linear Polymers. *ACS Macro Lett.* **2021**, *10*, 129−134.
(24) Chubak, I.; Pachong, S. M.; Kremer, K.; Likos, C. N.; Smrek, J. Active Topological Glass Confined within a Spherical Cavity. *Macromolecules* **2022**, *55*, 956−964.
(25) Böhmer, R.; Hinze, G.; Diezemann, G.; Geil, B.; Sillescu, H. Dynamic Heterogeneity in Supercooled Ortho-Terphenyl Studied by Multidimensional Deuteron NMR. *Europhys. Lett.* **1996**, *36*, 55−60.
(26) Richert, R.; Richert, M. Dynamic Heterogeneity, Spatially Distributed Stretched-Exponential Patterns, and Transient Dispersions in Solvation Dynamics. *Phys. Rev. E* **1998**, *58*, 779−784.
(27) Ediger, M. D. Spatially Heterogeneous Dynamics in Supercooled Liquids. *Annu. Rev. Phys. Chem.* **2000**, *51*, 99−128.
(28) Hurley, M. M.; Harrowell, P. Kinetic Structure of a Two-Dimensional Liquid. *Phys. Rev. E* **1995**, *52*, 1694−1698.
(29) Kob, W.; Donati, C.; Plimpton, S. J.; Poole, P. H.; Glotzer, S. C. Dynamical Heterogeneities in a Supercooled Lennard-Jones Liquid. *Phys. Rev. Lett.* **1997**, *79*, 2827−2830.
(30) Yamamoto, R.; Onuki, A. Kinetic Heterogeneities in a Highly Supercooled Liquid. *J. Phys. Soc. Jpn.* **1997**, *66*, 2545−2548.
(31) Donati, C.; Douglas, J. F.; Kob, W.; Plimpton, S. J.; Poole, P. H.; Glotzer, S. C. Stringlike Cooperative Motion in a Supercooled Liquid. *Phys. Rev. Lett.* **1998**, *80*, 2338−2341.
(32) Hurley, M. M.; Harrowell, P. Non-Gaussian Behavior and the Dynamical Complexity of Particle Motion in a Dense Two-dimensional Liquid. *J. Chem. Phys.* **1996**, *105*, 10521−10526.
(33) Shell, M. S.; Debenedetti, P. G.; Stillinger, F. H. Dynamic Heterogeneity and Non-Gaussian Behaviour in a Model Supercooled Liquid. *J. Phys.: Condens. Matter* **2005**, *17*, S4035−S4046.
(34) Flenner, E.; Szamel, G. Relaxation in a Glassy Binary Mixture: Comparison of the Mode-Coupling Theory to a Brownian Dynamics Simulation. *Phys. Rev. E* **2005**, *72*, 031508.
(35) Saltzman, E. J.; Schweizer, K. S. Non-Gaussian Effects, Space-Time Decoupling, and Mobility Bifurcation in Glassy Hard-Sphere Fluids and Suspensions. *Phys. Rev. E* **2006**, *74*, 061501.
(36) Chaudhuri, P.; Berthier, L.; Kob, W. Universal Nature of Particle Displacements Close to Glass and Jamming Transitions. *Phys. Rev. Lett.* **2007**, *99*, 060604.
(37) Aichele, M.; Gebremichael, Y.; Starr, F. W.; Baschnagel, J.; Glotzer, S. C. Polymer-Specific Effects of Bulk Relaxation and Stringlike Correlated Motion in the Dynamics of a Supercooled Polymer Melt. *J. Chem. Phys.* **2003**, *119*, 5290−5304.
(38) Peter, S.; Meyer, H.; Baschnagel, J. MD Simulation of Concentrated Polymer Solutions: Structural Relaxation near the Glass Transition. *Eur. Phys. J. E* **2009**, *28*, 147−158.
(39) Pan, D.; Sun, Z.-Y. Diffusion and Relaxation Dynamics of Supercooled Polymer Melts. *Chin. J. Polym. Sci.* **2018**, *36*, 1187−1194.
(40) Goto, S.; Kim, K.; Matubayasi, N. Effects of Chain Length on Rouse Modes and Non-Gaussianity in Linear and Ring Polymer Melts. *J. Chem. Phys.* **2021**, *155*, 124901.
(41) Slimani, M. Z.; Bacova, P.; Bernabei, M.; Narros, A.; Likos, C. N.; Moreno, A. J. Cluster Glasses of Semiflexible Ring Polymers. *ACS Macro Lett.* **2014**, *3*, 611−616.
(42) Brás, A. R.; Gooßen, S.; Krutyeva, M.; Radulescu, A.; Farago, B.; Allgaier, J.; Pyckhout-Hintzen, W.; Wischnewski, A.; Richter, D. Compact Structure and Non-Gaussian Dynamics of Ring Polymer Melts. *Soft Matter* **2014**, *10*, 3649−3655.
(43) Roy, P. K.; Chaudhuri, P.; Vemparala, S. Effect of Ring Stiffness and Ambient Pressure on the Dynamical Slowdown in Ring Polymers. *Soft Matter* **2022**, *18*, 2959−2967.
(44) Halverson, J. D.; Lee, W. B.; Grest, G. S.; Grosberg, A. Y.; Kremer, K. Molecular Dynamics Simulation Study of Nonconcatenated Ring Polymers in a Melt. I. Statics. *J. Chem. Phys.* **2011**, *134*, 204904.
(45) Halverson, J. D.; Lee, W. B.; Grest, G. S.; Grosberg, A. Y.; Kremer, K. Molecular Dynamics Simulation Study of Nonconcatenated Ring Polymers in a Melt. II. Dynamics. *J. Chem. Phys.* **2011**, *134*, 204905.
(46) Halverson, J. D.; Grest, G. S.; Grosberg, A. Y.; Kremer, K. Rheology of Ring Polymer Melts: From Linear Contaminants to Ring-Linear Blends. *Phys. Rev. Lett.* **2012**, *108*, 038301.
(47) Kremer, K.; Grest, G. S. Dynamics of Entangled Linear Polymer Melts: A Molecular-dynamics Simulation. *J. Chem. Phys.* **1990**, *92*, 5057−5086.
(48) Plimpton, S. Fast Parallel Algorithms for Short-Range Molecular Dynamics. *J. Comput. Phys.* **1995**, *117*, 1−19.



https://doi.org/10.1021/acspolymersau.3c00013
*ACS Polym. Au* 2023, 3, 437−446

(49) Hsu, H.-P.; Kremer, K. Static and Dynamic Properties of Large Polymer Melts in Equilibrium. *J. Chem. Phys.* **2016**, *144*, 154907.
(50) Hsu, H.-P.; Kremer, K. Detailed Analysis of Rouse Mode and Dynamic Scattering Function of Highly Entangled Polymer Melts in Equilibrium. *Eur. Phys. J. Spec. Top.* **2017**, *226*, 693−703.
(51) Parisi, D.; Costanzo, S.; Jeong, Y.; Ahn, J.; Chang, T.; Vlassopoulos, D.; Halverson, J. D.; Kremer, K.; Ge, T.; Rubinstein, M.; Grest, G. S.; Srinin, W.; Grosberg, A. Y. Nonlinear Shear Rheology of Entangled Polymer Rings. *Macromolecules* **2021**, *54*, 2811−2827.
(52) Tu, M. Q.; Davydovich, O.; Mei, B.; Singh, P. K.; Grest, G. S.; Schweizer, K. S.; O'Connor, T. C.; Schroeder, C. M. Unexpected Slow Relaxation Dynamics in Pure Ring Polymers Arise from Intermolecular Interactions. *ACS Polym. Au* **2023**, *3*, 307.
(53) Faller, R.; Kolb, A.; Müller-Plathe, F. Local Chain Ordering in Amorphous Polymer Melts: Influence of Chain Stiffness. *Phys. Chem. Chem. Phys.* **1999**, *1*, 2071−2076.
(54) Sukumaran, S. K.; Grest, G. S.; Kremer, K.; Everaers, R. Identifying the Primitive Path Mesh in Entangled Polymer Liquids. *J. Polym. Sci. B Polym. Phys.* **2005**, *43*, 917−933.
(55) Hagita, K.; Murashima, T. Effect of Chain-Penetration on Ring Shape for Mixtures of Rings and Linear Polymers. *Polymer* **2021**, *218*, 123493.
(56) Everaers, R.; Sukumaran, S. K.; Grest, G. S.; Svaneborg, C.; Sivasubramanian, A.; Kremer, K. Rheology and Microscopic Topology of Entangled Polymeric Liquids. *Science* **2004**, *303*, 823−826.
(57) Aronovitz, J.; Nelson, D. Universal Features of Polymer Shapes. *J. Phys. (Paris)* **1986**, *47*, 1445−1456.
(58) Rudnick, J.; Gaspari, G. The Asphericity of Random Walks. *J. Phys. A: Math. Gen.* **1986**, *19*, L191.
(59) Gaspari, G.; Rudnick, J.; Beldjenna, A. The Shapes of Open and Closed Random Walks: A 1/d Expansion. *J. Phys. A: Math. Gen.* **1987**, *20*, 3393.
(60) Jagodzinski, O.; Eisenriegler, E.; Kremer, K. Universal Shape Properties of Open and Closed Polymer Chains: Renormalization Group Analysis and Monte Carlo Experiments. *J. Phys. I France* **1992**, *2*, 2243−2279.
(61) Bishop, M.; Michels, J. P. J. The Shape of Ring Polymers. *J. Chem. Phys.* **1985**, *82*, 1059−1061.
(62) Bishop, M.; Saltiel, C. J. Polymer Shapes in Two, Four, and Five Dimensions. *J. Chem. Phys.* **1988**, *88*, 3976−3980.
(63) Zifferer, G.; Preusser, W. Monte Carlo Simulation Studies of the Size and Shape of Ring Polymers. *Macromol. Theory Simul.* **2001**, *10*, 397−407.
(64) Alim, K.; Frey, E. Shapes of Semiflexible Polymer Rings. *Phys. Rev. Lett.* **2007**, *99*, 198102.
(65) Rawdon, E. J.; Kern, J. C.; Piatek, M.; Plunkett, P.; Stasiak, A.; Millett, K. C. Effect of Knotting on the Shape of Polymers. *Macromolecules* **2008**, *41*, 8281−8287.
(66) Reigh, S. Y.; Yoon, D. Y. Concentration Dependence of Ring Polymer Conformations from Monte Carlo Simulations. *ACS Macro Lett.* **2013**, *2*, 296−300.
(67) Cai, X.; Liang, C.; Liu, H.; Zhang, G. Conformation and Structure of Ring Polymers in Semidilute Solutions: A Molecular Dynamics Simulation Study. *Polymer* **2022**, *253*, 124953.
(68) Bernabei, M.; Bacova, P.; Moreno, A. J.; Narros, A.; Likos, C. N. Fluids of semiflexible ring polymers: effective potentials and clustering. *Soft Matter* **2013**, *9*, 1287−1300.
(69) Michieletto, D.; Marenduzzo, D.; Orlandini, E. Is the Kinetoplast DNA a Percolating Network of Linked Rings at Its Critical Point? *Phys. Biol.* **2015**, *12*, 036001.
(70) Yamamoto, R.; Onuki, A. Dynamics of Highly Supercooled Liquids: Heterogeneity, Rheology, and Diffusion. *Phys. Rev. E* **1998**, *58*, 3515−3529.
(71) Shiba, H.; Kawasaki, T.; Onuki, A. Relationship between Bond-Breakage Correlations and Four-Point Correlations in Heterogeneous Glassy Dynamics: Configuration Changes and Vibration Modes. *Phys. Rev. E* **2012**, *86*, 041504.
(72) Kawasaki, T.; Onuki, A. Slow Relaxations and Stringlike Jump Motions in Fragile Glass-Forming Liquids: Breakdown of the Stokes-Einstein Relation. *Phys. Rev. E* **2013**, *87*, 012312.
(73) Shiba, H.; Yamada, Y.; Kawasaki, T.; Kim, K. Unveiling Dimensionality Dependence of Glassy Dynamics: 2D Infinite Fluctuation Eclipses Inherent Structural Relaxation. *Phys. Rev. Lett.* **2016**, *117*, 245701.
(74) Dell, Z. E.; Schweizer, K. S. Intermolecular Structural Correlations in Model Globular and Unconcatenated Ring Polymer Liquids. *Soft Matter* **2018**, *14*, 9132−9142.
(75) Mei, B.; Dell, Z. E.; Schweizer, K. S. Microscopic Theory of Long-Time Center-of-Mass Self-Diffusion and Anomalous Transport in Ring Polymer Liquids. *Macromolecules* **2020**, *53*, 10431−10445.
(76) Mei, B.; Dell, Z. E.; Schweizer, K. S. Theory of Transient Localization, Activated Dynamics, and a Macromolecular Glass Transition in Ring Polymer Liquids. *ACS Macro Lett.* **2021**, *10*, 1229−1235.
(77) Jeong, C.; Douglas, J. F. Relation between Polymer Conformational Structure and Dynamics in Linear and Ring Polyethylene Blends. *Macromol. Theory Simul.* **2017**, *26*, 1700045.
(78) Borger, A.; Wang, W.; O'Connor, T. C.; Ge, T.; Grest, G. S.; Jensen, G. V.; Ahn, J.; Chang, T.; Hassager, O.; Mortensen, K.; Vlassopoulos, D.; Huang, Q. Threading−Unthreading Transition of Linear-Ring Polymer Blends in Extensional Flow. *ACS Macro Lett.* **2020**, *9*, 1452−1457.
(79) O'Connor, T. C.; Ge, T.; Grest, G. S. Composite Entanglement Topology and Extensional Rheology of Symmetric Ring-Linear Polymer Blends. *J. Rheol.* **2022**, *66*, 49−65.
(80) Grest, G. S.; Ge, T.; Plimpton, S. J.; Rubinstein, M.; O'Connor, T. C. Entropic Mixing of Ring/Linear Polymer Blends. *ACS Polym. Au* **2023**, *3*, 209−216.


https://doi.org/10.1021/acspolymersau.3c00013
*ACS Polym. Au* 2023, 3, 437−446